Inorganic Chemistry

Article

pubs.acs.org/IC

# Tuning of Valence States, Bonding Types, Hierarchical Structures, and Physical Properties in Copper/Halide/Isonicotinate System

Min-Min Liu, Juan-Juan Hou, Zhi-kai Qi, Li−Na Duan, Wen-Juan Ji, Cai-yun Han, and Xian-Ming Zhang*

School of Chemistry & Material Science, Shanxi Normal University Linfen 041004, P. R. China

Supporting Information

**ABSTRACT:** Seven cupric halide coordination polymers, namely $[Cu_5(OH)_3Br_3(ina)_4]$ (**1**), $[Cu_5(OH)_3Cl_3(ina)_4]$ (**2**), $[Cu_2(OH)Cl(ina)_2]$ (**3**), $[Cu_3(OH)_2Cl_2(ina)_2]\cdot 2H_2O$ (**4**), $[Cu_3(OH)_2Br_2(ina)_2]\cdot 2H_2O$ (**5**), $[Cu_2Cl_2(ina)_2(H_2O)_2]$ (**6**), $[Cu_2Cl(ina)_2(gca)(H_2O)]$ (**7**), cupric complex templated cuprous halide $[Cu^{II}(Me\text{-}ina)_2(H_2O)]\text{-}[Cu^{I}_5Br_7]$ (**8**), and organic templated cuprous halide $Me_2\text{-}ina[Cu_2Br_3]$ (**9**) (Hina = isonicotinic acid), were prepared from the starting materials of cupric halide and Hina via fine-tuning solvothermal reactions. According to valence states of copper, **1**−**7** are copper(II) complexes, **8** is a mixed-valent Cu(I,II) complex, while **9** is a Cu(I) compound. According to bonding types of halides, nine complexes can be classified as three types: complexes **1**−**3** include only normal X−Cu bond (X = halide); complexes **4**−**7** include normal X−Cu bond and X···Cu weak bond; complexes **8** and **9** include normal X−Cu bond and X···H−C halogen hydrogen bonds. Complexes **1** and **2** are isomorphic three-dimensional (3D) pcu topological metal organic frameworks (MOFs) with butterfly-like $Cu_4(\mu_3\text{-}OH)_2X_2$ and steplike $Cu_6(\mu_3\text{-}OH)_4$ cores as nodes, showing strong ferromagnetic couplings. Complex **3** also is a pcu topological MOF with only butterfly-like $Cu_4(\mu_3\text{-}OH)_2Cl_2$ clusters as nodes, presenting spin canting antiferromagnetic behavior. Isostructural **4** and **5** are $Cu_3(OH)_2$ clusters based two-dimensional (2D) (4,4) layers, which are extended into 3D eight-connected networks via weak Cu···X bonds, showing ferromagnetic coupling. Antiferromagnetic **6** is a simple one-dimensional coordination polymer, which is extended via weak Cu···Cl bonds into 3D (3,4)-connected networks. Paramagnetic **7** is a ladderlike polymer, which is extended into 2D (3,4)-connected layer via weak Cu···Cl bonds. The syntheses of polymeric cupric complexes **1**−**7** mainly result from differences in reactant ratio and pH value. Utilization of reducing methanol generated novel cubane-containing $[Cu_5Br_7]^{2-}$ chain templated by paddlewheel-like $[Cu^{II}(Me\text{-}ina)_2]^{2+}$ **8** and face-shared dimer-containing $[Cu_2Br_3]^{-}$ chain templated by N-methylated and O-esterificated $Me_2$-ina **9**. Complex **9** exhibits a strong red emission and a weaker green emission upon excitation.

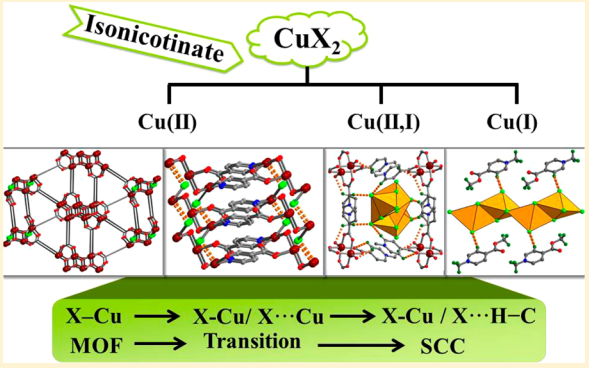


## INTRODUCTION

Crystal engineering of metal−organic materials (MOMs) with functional secondary building units (SBUs), in a position to be divided into metal−organic frameworks (MOFs) and supramolecular coordination complexes (SCCs) on the most basic level, may generate diverse structures with tunable properties.[1] Because of the varied stereochemistry of copper atoms and the different redox potentials among Cu(II), Cu(I,II), and Cu(I) ions, construction of various MOMs with aesthetically pleasing structures by polynuclear copper clusters as SBUs continues to attract considerable interest in molecular nanoscience such as magnetism, luminescence, and photocatalysis.[2] The in situ modulation of copper clusters and their connectivity proves more challenging in the rationalization of network topology and improvement of properties for multifunctional MOMs.[3]

The $d^9$ configuration of Cu(II) ion is subject to dynamic Jahn−Teller distortion in all its stereochemistry, especially if placed in an environment of cubic (regular octahedral or tetrahedral) symmetry.[4] Therefore, Cu(II) ions can offer unique characteristics (i.e., normal weak, weak bond, coordination flexibility, polarity, and Lewis acid) as metal centers of functional MOMs.[5] The flexible and versatile Cu(II) coordination spheres play a vital role in creating new tunable frameworks, which can be realized by the changes in coordination numbers as a result of an alternative means of lifting the degeneracy of unequally occupied d orbitals.[6] The Jahn−Teller distortion at the axial sites can promote the generation of "4 + 1"or "4 + 2" coordination geometry for Cu(II) ions, resulting in weak Cu···X bonds (X = halide). These Cu···X bonds are weaker than normal coordination bonds but are stronger than intermolecular interactions, which take an important part in the formation of hierarchical supramolecular structure. According to the soft and hard acids and bases theory, the coordinately flexible Lewis acid Cu(II) ions in combination with moderate Lewis bases of Cl and Br ions can be preferentially coordinated by carboxylate and

**Received:** January 22, 2014
**Published:** April 8, 2014

   dx.doi.org/10.1021/ic5001232 | *Inorg. Chem.* 2014, 53, 4130−4143

hydroxyl Lewis base groups to generate cupric clusters based on Cu−O/X−Cu connectivity.[7] The choice and design of different kinds of SBUs based on cupric clusters, that is, paddlewheel-like $Cu_2$ units,[8] linear and triangular $Cu_3$ units,[9] butterfly and cubane $Cu_4$ units,[10] stepped $Cu_8$ units,[11] and so on, enables the fine-tuning of MOMs, especially for magnetism.[12] With cupric clusters as "magnetic bricks," superexchange interactions are correlated with Cu···Cu distances, Cu−O/X−Cu angles, and local geometries of copper atoms.[13]

The Cu(II) salts are stable at ambient conditions either in solution or solid state. The tendency of Cu(II)-to-Cu(I) reduction at room temperature can be promoted by increase of reaction temperature or incorporation of reducing solvent.[14] The relative stabilities of Cu(I) and Cu(II) states in aqueous solution also depend very strongly on ligands or the nature of neighboring atoms in a crystal. Studies have shown that Cu(II) can be solvothermally converted into Cu(I) in the presence of different heterocyclic species.[15] For example, with the auxiliary of polydentate *N*-heterocycle ligands such as pyrazine, imidazole, pyridine, and 1,4-diazabicyclo[2.2.2]octane (DABCO), cuprous CuX-based aggregates are accessible from Cu(II) salts as starting materials, which have been widely used as luminescent or photocatalytic MOMs in the presence of intramolecular hydrogen bonding, $\pi-\pi$ stacking interactions, van der Waals forces, and other weak interactions. Therefore, in situ reduction of Cu(II) salts can be an effective method to access mixed-valent Cu(I,II) and cuprous Cu(I) MOMs.[16] Different from copper(II), ranging from four-coordinate square planar to eight-coordinate distorted dodecahedron, copper(I) ions usually possess typical coordination geometries from linearity and triangle to tetrahedron. Nevertheless, structural diversity of CuX-based coordination polymers can not only depend on the copper(I) ions but also on the halide anions of strongly coordinated nature. It is revealed that halide anions can act as terminal, $\mu_2$, $\mu_3$, and even $\mu_8$ mode to connect copper(I) ions. Most anionic copper(I) halide aggregates exist as isolated complexes such as clusters and one-dimensional (1D) chains, nearly all of which are derived from three simple synthons of linear $CuX_2$, planar triangular $CuX_3$, and tetrahedral $CuX_4$ via corner/edge/face-sharing modes.[2b] Since most $(Cu_xX_y)^{x-y}$ $(x < y)$ aggregates are anionic, the key factor to modulate their structures is direct addition of organic amines with opposite charges.[17] However, several cooperative in situ solvothermal reactions including alkylation, desulfurization, and cycloaddition occurred in the Cu(II)-to-Cu(I) reduction process, which provides an alternative indirect template approach to design and synthesize novel cuprous or mixed-valent copper MOMs.[18] Otherwise, the anionic $(Cu_xX_y)^{x-y}$ aggregates can generate crystal packing by electrostatic interaction and C−H···X interactions with alkyl/aryl polyatomic cationic templates of in situ solvothermal reactions.

Previous reports have shown that pyridyl carboxylates such as isonicotinic acid (Hina) tend to bind metal centers with both pyridyl and carboxylate groups to form extended networks, where carboxylate groups balance the metal charges.[19] However, recent studies indicate that the pyridyl nitrogen and the carboxylate oxygen in ina can be in situ R-alkylated and RR′-esterificated to form R-ina and RR′-ina templates for novel MOMs.[20] Furthermore, singly alkylated R-ina group is a zwitterion, which could also be utilized as both template and ligand to form MOMs.

In this Report, by carefully varying the ratio of starting materials and the amount of modulating reagent, nine complexes, including seven cupric cluster-based MOFs with Cu−O/X-Cu connectivity, one mixed-valent Cu(I,II), and one cuprous SCC, namely $[Cu_5(OH)_3Br_3(ina)_4]$ (**1**), $[Cu_5(OH)_3Cl_3(ina)_4]$ (**2**), $[Cu_2(OH)Cl(ina)_2]$ (**3**), $[Cu_3(OH)_2Cl_2(ina)_2]\cdot 2H_2O$ (**4**), $[Cu_3(OH)_2Br_2(ina)_2]\cdot 2H_2O$ (**5**), $[Cu_2Cl_2(ina)_2(H_2O)_2]$ (**6**), $[Cu_2Cl(ina)_2(gca)(H_2O)]$ (**7**), $[Cu^{II}(Me\text{-}ina)_2(H_2O)][Cu^{I}_5Br_7]$ (**8**), and $Me_2$-ina$[Cu_2Br_3]$ (**9**), were prepared from copper halides and isonicotinic acid under tunable solvothermal conditions. Regular changes of valence states of copper, bonding types of halides, hierarchical structures, and physical properties were observed.

## EXPERIMENTAL SECTION

**Materials and Physical Measurements.** All chemicals were analytically pure from commercial sources and used without further purification. Elemental analyses were performed on a Vario EL-II analyzer. Fourier transform infrared (FTIR) spectra were recorded from KBr pellets in the range of 4000−400 $cm^{-1}$ on a Perkin-Elmer Spectrum BX FT-IR spectrometer. Powder X-ray diffraction (PXRD) data were collected in a Rigaku Ultima IV diffractometer. The magnetic measurements were studied with Quantum Design SQUID MPMS XL-5 instrument. The diamagnetic correction for each sample was applied using Pascal's constants. Photoluminescence analyses were performed on an Edinburgh FLS920 luminescence spectrometer.

**Syntheses.** *$[Cu_5(OH)_3Br_3(ina)_4]$ (**1**).* A mixture of $CuBr_2$ (0.089 g, 0.4 mmol), Hina (0.037 g, 0.30 mmol), NaOH (0.12 g, 0.30 mmol), MeCN (3 mL), and $H_2O$ (2 mL) in the molar ratio of 4:3:3:571:1111 was stirred, then sealed in a 12 mL Teflon-lined stainless autoclave and heated to 130 °C for 5 d. After it was cooled to room temperature and subjected to filtration, green block crystals of **1** were recovered in 71.5% yield. Anal. Calcd (%) for $C_{24}H_{19}Br_3Cu_5N_4O_{11}$: C, 26.28; H, 1.73; N, 5.11. Found: C, 25.94; H, 1.52; N, 4.87. IR data (KBr, $cm^{-1}$): 3406(s), 1645(s), 1609(s), 1538(s), 688(m), 1241(w), 1050(w), 950(w), 785(w), 609(w), 506(w).

*$[Cu_5(OH)_3Cl_3(ina)_4]$ (**2**).* The synthetic procedure is similar to that of **1**, except that the metal source is $CuCl_2$. Light green block crystals of **2** in yield of 50.9% were recovered. Anal. Calcd (%) for $C_{24}H_{19}Cl_3Cu_5N_4O_{11}$: C, 29.92; H, 1.97.; N, 5.81. Found: C, 28.91; H, 1.72; N, 5.66. IR data (KBr, $cm^{-1}$): 3412(s), 1650(s), 1611(s), 1535(s), 695(m), 1231(w), 1038(w), 939(w), 780(w), 613(w), 501(w).

*$[Cu_2(OH)Cl(ina)_2]$ (**3**).* A mixture of $CuCl_2$ (0.119 g, 0.7 mmol), ina (0.064 g, 0.50 mmol), ox (0.018 g, 0.20 mmol) (ox = oxalic acid), NaOH (0.020 g, 0.50 mmol), MeCN (5 mL), and $H_2O$ (3 mL) in the molar ratio of 7:5:2:951:1667 was stirred, then sealed in a 25 mL Teflon-lined stainless autoclave and heated to 130 °C for 5 d. After it was cooled to room temperature and subjected to filtration, green block crystals of **3** were recovered in 63.5% yield. Anal. Calcd (%) for $C_{12}H_8ClCu_2N_2O_5$: C, 34.06; H, 1.89.; N, 6.62. Found: C, 33.84; H, 1.65; N, 6.43. IR data (KBr, $cm^{-1}$): 3437(s), 1609(s), 1546(s), 1370(s), 688(m), 697(m), 3085(w), 1210(w), 905(w), 785(w), 544(w), 445(w).

*$[Cu_3Cl_2(OH)_2(ina)_2]\cdot 2H_2O$ (**4**).* The synthetic procedure is similar to that of **2**, except that the amount of NaOH is 0.20 mmol. Blue sheet crystals of **4** in yield of 70.2% were recovered. Anal. Calcd (%) for $C_{12}H_{14}Cl_2Cu_3N_2O_8$: C, 25.01; H, 2.43; N, 4.87. Found: C, 24.79; H, 2.52; N, 4.51. IR data (KBr, $cm^{-1}$): 3429(s), 1650(s), 1603(s), 1415(s), 1361(s), 1546(m), 2916(w), 1043(w), 952(w), 754(w), 697(w).

*$[Cu_3Br_2(OH)_2(ina)_2]\cdot 2H_2O$ (**5**).* The synthetic procedure is similar to that of **4**, except that the metal source is $CuBr_2$. Green sheet crystals of **5** in yield of 65.2% were recovered. Anal. Calcd (%) for $C_{12}H_{14}Br_2Cu_3N_2O_8$: C, 21.73; H, 2.12; N, 4.23. Found: C, 21.48; H, 2.43; N, 3.89. IR data (KBr, $cm^{-1}$): 3388(s), 1659(s), 1608(s), 1413 (s), 1358(s), 1546(m), 2908(w), 1032(w), 948(w), 759(w), 692(w).

*$[Cu_2Cl_2(ina)_2(H_2O)_2]$ (**6**).* The synthetic procedure is similar to that of **2** except for using $[N(Me)_4]Cl$ (0.033 g, 0.2 mmol) instead of NaOH; blue sheet crystals of **6** in yield of 86% were recovered. Anal. Calcd (%) for $C_{12}Cl_2Cu_2N_2O_6H_{12}$: C, 30.11; H, 2.51; N, 5.86. Found: C, 30.02; H, 2.42; N, 5.77. IR data (KBr, $cm^{-1}$): 3378(s), 1607(s), 1556(s), 1472(s), 688(s), 776(m), 1235(w), 1153(w), 1041(w), 950(w), 873(w), 465(w).


dx.doi.org/10.1021/ic5001232 | *Inorg. Chem.* 2014, 53, 4130−4143

Table 1. Crystal Data and Structure Refinement for Complexes 1−3

| complex | 1 | 2 | 3 |
|---|---|---|---|
| empirical formula | $C_{24}H_{19}Br_3Cu_5N_4O_{11}$ | $C_{24}H_{19}Cl_3Cu_5N_4O_{11}$ | $C_{12}H_8ClCu_2N_2O_5$ |
| formula weight | 1096.86 | 963.48 | 422.73 |
| temperature | 298(2) K | 298(2) K | 298(2) K |
| crystal system | triclinic | triclinic | monoclinic |
| space group | $P\bar{1}$ | $P\bar{1}$ | $P2_1/n$ |
| $a$ (Å) | 6.1549(12) | 5.951(7) | 6.1018(2) |
| $b$ (Å) | 10.678(2) | 10.706(11) | 21.6019(6) |
| $c$ (Å) | 25.259(5) | 25.35(3) | 11.0266(3) |
| $\alpha$ (deg) | 91.801(4) | 90.92(2) | 90 |
| $\beta$ (deg) | 90.600(4) | 90.37(2) | 105.0430(10) |
| $\gamma$ (deg) | 102.554(4) | 101.89(2) | 90 |
| $V$ (Å$^3$) | 1619.4(6) | 1580(3) | 1403.61(7) |
| $Z$ | 2 | 2 | 4 |
| $\rho_{calc}$, (g cm$^{-3}$) | 2.249 | 2.025 | 2.000 |
| $\mu$, (mm$^{-1}$) | 6.993 | 3.626 | 3.244 |
| F(000) | 1058 | 950 | 836 |
| size (mm) | 0.22 × 0.18 × 0.16 | 0.20 × 0.16 × 0.14 | 0.26 × 0.24 × 0.22 |
| $\theta$ (deg) | 1.61 to 24.87 | 1.61 to 25.00 | 2.13 to 27.00 |
| reflections/unique | 6595/5283 | 6608/5262 | 8656/3039 |
| $T_{max}/T_{min}$ | 0.4008/0.3084 | 0.6307/0.5308 | 0.5355/0.4859 |
| data/parameters | 5283/0/424 | 5262/0/424 | 3039/0/199 |
| $S$ | 1.044 | 1.027 | 1.069 |
| $R_1{}^a$, $wR_2{}^b$ [$I > 2\sigma(I)$] | 0.0491, 0.1387 | 0.0683, 0.1384 | 0.0211, 0.0557 |
| $R_1{}^a$, $wR_2{}^b$ (all data) | 0.0664, 0.1728 | 0.1996, 0.1535 | 0.0225, 0.0566 |
| $\Delta\rho$max/$\Delta\rho$min (e Å$^{-3}$) | 1.15/−1.10 | 0.92/−0.96 | 0.748/−0.408 |

$^a R_1 = F_o - F_c/F_o$. $^b wR_2 = [w(F_o^2 - F_c^2)^2/w(F_o^2)^2]^{1/2}$

*[$Cu_2Cl(ina)_2(gca)(H_2O)$] (**7**).* The synthetic procedure is similar to that of **3** except for using Hgca (0.023 g, 0.20 mmol) (Hgca = hydroxyacetic acid) instead of ox (0.018 g, 0.20 mmol); dark blue block crystals of **7** were recovered in 75% yield. Anal. Calcd (%) for $C_{14}O_8N_2ClCu_2H_{13}$: C, 33.61; H, 2.60. N, 5.60. Found: C, 33.50; H, 2.48; N, 5.49. IR data (KBr, cm$^{-1}$): 3268(s), 1659(s), 1562(s), 1470(s), 1323(s), 688(s), 1226(m), 1090(m), 2916(w), 1018(w), 875(w), 785(w), 562(w).

*[$Cu^{II}(Me\text{-}ina)_2(H_2O)][Cu^{I}{}_5Br_7$](**8**).* A mixture of $CuBr_2$ (0.223 g, 1.0 mmol), ina (0.025 g, 0.20 mmol), 2,2-dimethylolpropionic acid (0.067 g, 0.50 mmol), NaOH (0.018 g, 0.45 mmol), MeOH (4 mL), and $H_2O$ (2.5 mL) in the molar ratio of 100:20:50:45:9888:13889 was stirred, then sealed in a 12 mL Teflon-lined stainless autoclave and heated to 130 °C for 5 d. After it was cooled to room temperature and subjected to filtration, black block crystals of **8** were recovered in 71.5% yield. Anal. Calcd (%) for $C_{14}H_{16}Br_7Cu_6\ N_2O_5$: C,13.65; H, 1.31; N, 2.27. Found: C, 13.53; H, 1.07; N, 2.18. IR data (KBr, cm$^{-1}$): 3453(s), 1659(s), 1571(s), 1411(s), 1282(m), 770(m), 3045(w), 2925(m), 2844(w), 873(w), 641(w), 465(w).

*$Me_2$-ina[$Cu_2Br_3$] (**9**).* The synthetic procedure of **9** is similar to that of **8**, except the solvent is pure MeOH (6 mL). Red block crystals of **9** in yield of 87% were recovered. Anal. Calcd (%) for $C_7H_7Br_3Cu_2NO_2$: C, 16.19; H, 1.35; N, 2.70. Found: C, 15.53; H, 1.15; N, 2.18. IR data (KBr, cm$^{-1}$): 3453(s), 1731(s), 1298(s), 1417(m), 1125(m), 3061(w), 2932(s), 1571 (s), 946(w), 873(w), 761(w), 673(w).

**X-ray Data Collection and Structure Determination.** Data collection was performed with Mo K$\alpha$ radiation ($\lambda$ = 0.710 73 Å) on a Bruker Apex CCD diffractometer at 298(2) K for complexes **1**−**9**. The SAINT program was used for integration of the diffraction profiles, and the SADABS program was used for X absorption correction. All the structures were solved by direct methods using the SHELXS program and refined by full-matrix least-squares methods with SHELXL. All non-hydrogen atoms were refined with anisotropic thermal parameters. Hydrogen atoms of organic ligands were generated theoretically onto the specific carbon and nitrogen atoms and were refined isotropically with fixed thermal factors. The hydrogen atoms of the water molecules were calculated by Platon software. Further details for structural analysis are summarized in Tables 1−3, and selected bond lengths and bond angles are shown in Supporting Information, Table S1.

## RESULTS AND DISCUSSION

**Synthesis Chemistry.** The reaction of cupric halides ($CuCl_2$ and $CuBr_2$) and Hina under solvothermal conditions gave seven magnetic cupric complexes **1**−**7**, one mixed-valent Cu(I,II) complex **8**, and one luminescent cuprous complex **9**. By systematically mediating pH value by adding NaOH and by introducing oxalic acid as auxiliary ligand, hydroxyl-containing SBUs such as butterfly-like $Cu_4(OH)_2X_2(CO_2)_2$, steplike $Cu_6(OH)_4(CO_2)_4$, and linear $Cu_3(OH)_2(CO_2)_2$ clusters were formed and assembled in complexes **1**−**5**. The variation of systemic pH can make a new complex **6**, which is found by using $[N(Me)_4]Cl$ instead of NaOH. The introduction of auxiliary hydroxyacetic acid can not only change the reaction pH value but also take part in the construction of **7**. Some related known complexes such as $[Cu_2Br(ina)_2]$ and $[Cu_2Cl(ina)]$ have been obtained during the syntheses of **1**−**7** via change of pH values,[21] which means that our synthesis method is general. Introduction of reducing solvent is very important in the process of in situ reduction of Cu(II) ions. Experimental results of complexes **8** and **9** revealed that the increase of temperature from 130 to 140 °C and the use of MeOH solvent in starting materials help to form mixed-valent Cu(I,II) and cuprous MOMs. In addtion to reducing reactant, methanol also has an important impact in the methylation and esterification of ina group in the formation of **8** and **9** under higher temperature and alkaline conditions. In situ N-methylation and O-esterification of ina group to form Me-ina and $Me_2$-ina in **8** and **9** was also proved by featured C−H stretching vibrations of the methyl groups (2932 cm$^{-1}$, 2925 cm$^{-1}$)


dx.doi.org/10.1021/ic5001232 | Inorg. Chem. 2014, 53, 4130−4143

**Table 2. Crystal Data and Structure Refinement for Complexes 4−7**

| complex | 4 | 5 | 6 | 7 |
|---|---|---|---|---|
| empirical formula | $C_{12}H_{14}Cl_2Cu_3N_2O_8$ | $C_{12}H_{12}Br_2Cu_3N_2O_8$ | $C_{12}H_{12}Cl_2Cu_2N_2O_6$ | $C_{14}H_{13}ClCu_2N_2O_8$ |
| formula weight | 575.77 | 662.68 | 478.22 | 499.79 |
| temperature | 298(2) K | 298(2) K | 298(2) K | 298(15) K |
| crystal system | monoclinic | monoclinic | triclinic | monoclinic |
| space group | $P2_1/c$ | $P2_1/c$ | $P\bar{1}$ | $P2_1/a$ |
| $a$ (Å) | 9.7398(5) | 9.693(9) | 7.5825(3) | 11.3747(4) |
| $b$ (Å) | 13.0223(6) | 13.192(13) | 10.5201(5) | 12.1459(4) |
| $c$ (Å) | 7.1713(3) | 7.432(7) | 11.2163(5) | 12.6348(5) |
| $\alpha$ (deg) | 90 | 90 | 108.0190(10) | 90.00 |
| $\beta$ (deg) | 105.4930(10) | 105.632(16) | 100.5900(10) | 92.6352(7) |
| $\gamma$ (deg) | 90 | 90 | 105.6750(10) | 90.00 |
| $V$ (Å$^3$) | 876.52(7) | 915.2(15) | 783.48(6) | 1743.73(11) |
| $Z$ | 2 | 2 | 2 | 4 |
| $\rho_{calc}$, (g cm$^{-3}$) | 1.946 | 2.405 | 2.027 | 1.904 |
| $\mu$, (mm$^{-1}$) | 3.944 | 7.864 | 3.088 | 2.639 |
| F(000) | 506 | 638 | 476 | 1000 |
| size (mm) | 0.22 × 0.16 × 0.12 | 0.22 × 0.16 × 0.12 | 0.16 × 0.12 × 0.08 | 0.48 × 0.36 × 0.20 |
| $\theta$ (deg) | 2.17 to 28.72 | 2.18 to 26.37 | 2.00 to 25.02 | 1.61 to 28.56 |
| reflections/unique | 3508/1520 | 4165/1861 | 4299/2742 | 6149/2933 |
| $T_{max}/T_{min}$ | 0.6332/0.3954 | 0.4589/0.2819 | 0.7903/0.6379 | 0.6203/0.3639 |
| data/parameters | 1520/0/124 | 1861/0/124 | 2742/0/219 | 2933/2/248 |
| S | 1.085 | 1.051 | 0.823 | 1. 065 |
| $R_1$[a], $wR_2$[b] [$I > 2\sigma(I)$] | 0.0268, 0.0777 | 0.0239, 0.0636 | 0.0334, 0.1014 | 0.0263, 0.0750 |
| $R_1$[a], $wR_2$[b] (all data) | 0.0296, 0.0803 | 0.0281, 0.0660 | 0.0385, 0.1086 | 0.0292, 0.0768 |
| $\Delta\rho$max/$\Delta\rho$min (e Å$^{-3}$) | 0.64/−0.61 | 0.68/−0.75 | 0.58/−0.314 | 0.53/−0.48 |

[a] $R_1 = F_o - F_c/F_o$. [b] $wR_2 = [w(F_o^2 - F_c^2)^2/w(F_o^2)^2]^{1/2}$

**Table 3. Crystal Data and Structure Refinement for Complexes 8 and 9**

| complex | 8 | 9 |
|---|---|---|
| empirical formula | $C_{14}H_{16}Br_7Cu_6N_2O_5$ | $C_8H_{10}Br_3Cu_2NO_2$ |
| formula weight | 1232.88 | 518.97 |
| temperature | 298(2) K | 298(2) K |
| crystal system | monoclinic | triclinic |
| space group | $P2_1/c$ | $P\bar{1}$ |
| $a$ (Å) | 11.007(3) | 7.9345(6) |
| $b$ (Å) | 22.483(5) | 8.6669(7) |
| $c$ (Å) | 12.325(3) | 10.4946(8) |
| $\alpha$ (deg) | 90 | 88.037(2) |
| $\beta$ (deg) | 98.604(5) | 72.8260(10) |
| $\gamma$ (deg) | 90 | 77.7960(10) |
| $V$ (Å$^3$) | 3015.8(12) | 673.62(9) |
| $Z$ | 4 | 1 |
| $\rho_{calc}$, (g cm$^{-3}$) | 2.711 | 2.559 |
| $\mu$, (mm$^{-1}$) | 13.456 | 12.037 |
| F(000) | 2284 | 488 |
| size (mm) | 0.22 × 0.17 × 0.12 | 0.18 × 0.14 × 0.12 |
| $\theta$ (deg) | 1.81 to 27 | 2.41 to 23.25 |
| reflections/unique | 14575/6463 | 2400/1856 |
| $T_{max}/T_{min}$ | 0.4124/0.1558 | 0.5355/0.2389 |
| data/parameters | 6463/0/317 | 1856/0/154 |
| S | 1.027 | 1.080 |
| $R_1$[a], $wR_2$[b] [$I > 2\sigma(I)$] | 0.0704, 0.2067 | 0.0747, 0.2257 |
| $R_1$[a], $wR_2$[b] (all data) | 0.1378, 0.2494 | 0.0883, 0.2452 |
| $\Delta\rho$max/$\Delta\rho$min (e Å$^{-3}$) | 2.97/−2.10 | 1.69/−1.51 |

[a] $R_1 = F_o$-$F_c/F_o$, [b] $wR_2 = [w(F_o^2$-$F_c^2)^2/w(F_o^2)^2]^{1/2}$

in IR spectra (Figure S1 in the Supporting Information). The purity of complexes **1**−**9** was confirmed by comparison of experimental PXRD patterns with the simulated pattern derived from the X-ray single-crystal data (Supporting Information, Figure S2).

**Descriptions of Crystal Structures.** Single-crystal X-ray diffraction analyses reveal that complex **1** crystallizes in the triclinic space group $P\bar{1}$, and the asymmetric unit consists of five crystallographically independent Cu(II) atoms, four ina groups, three $\mu_3$-OH groups and three bromides (Figure 1a). All five Cu(II) atoms occupy general position and show Jahn−Teller distorted coordination geometries. The Cu(1), Cu(3), and Cu(4) sites have similar distorted square pyramidal geometries, the Cu(2) site possesses a distorted octahedral geometry, and the Cu(5) site adopts a slightly distorted square geometry. The Cu(1) ion is coordinated by one $\mu_2$-Br atom, two $\mu_3$-$O_{hydroxyl}$ atoms, one bis(monodentate) carboxylate oxygen atom, and one pyridine nitrogen atom from two ina groups. The configuration of the Cu(2) site is formed by one $\mu_2$-Br atom, one $\mu_3$-$O_{hydroxyl}$ atom, two chelate carboxylate oxygen atoms, one bis(monodentate) carboxylate oxygen atom, and one pyridine nitrogen atom. The geometry of Cu(3) site is completed by one bromine atom, one $\mu_3$-$O_{hydroxyl}$ atom, two bis(monodentate) carboxylate oxygen atoms, and one pyridine nitrogen atom. The Cu(4) ion is ligated by one bromine atom, three $\mu_3$-$O_{hydroxyl}$ atoms, and one bis(monodentate) carboxylate oxygen atom. The coordination model of the Cu(5) site is constructed from two $\mu_3$-$O_{hydroxyl}$ atoms, one bis(monodentate) carboxylate atom, and one pyridine nitrogen atom. The Cu−O, Cu−N, and Cu−Br distances are in the range of 1.941(6)−2.252(6)Å, 1.988(8)−2.020(7)Å, and 2.4122(14)−2.7703(14) Å, respectively. The cis and trans angles of L−Cu(1)−L (L = O, N, and Br) are in the range of 78.34(17)−116.9(2)° and 140.4(3)−178.3(3)°. The Cu−O−Cu angles are in the range of 95.8(2)−126.7(3)°, and the Cu(2)−Br(1)−Cu(1) angle is 73.36(4)°.


dx.doi.org/10.1021/ic5001232 | Inorg. Chem. 2014, 53, 4130−4143

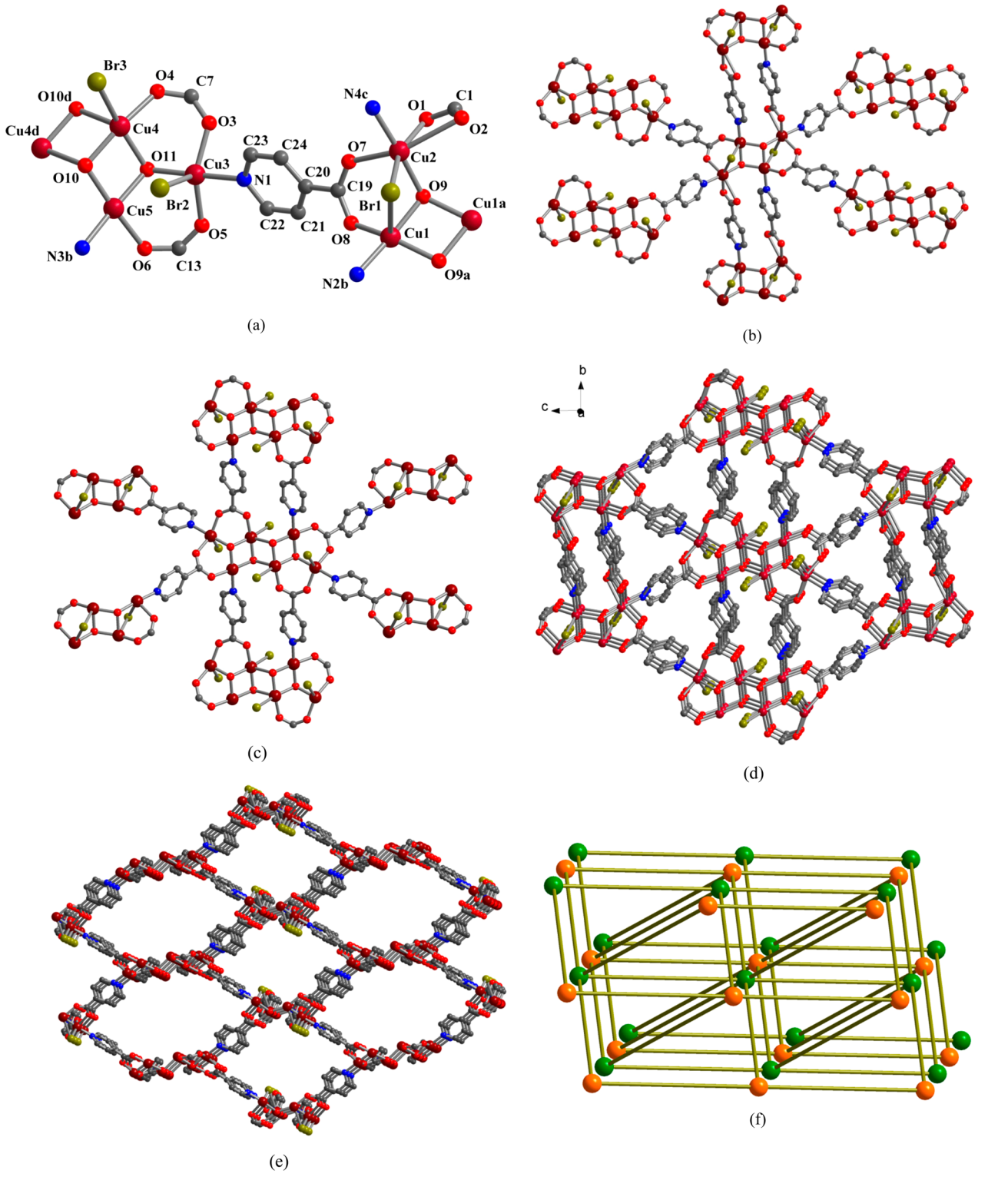


**Figure 1.** The coordination environment of Cu(II) ions (a), the connection modes of butterfly-like $Cu_4(OH)_2Br_2(CO_2)_2$ clusters (b), and steplike $Cu_6(OH)_4(CO_2)_4$ clusters (c), 3D hexagon framework with two types of pores at hkl = 2,9,0 (d, e) and pcu toplogical net (f) in complex **1**.

The two edge-shared Cu(1) and Cu(2) dimers, via $\mu_2$-Br atom and syn−syn carboxylate group, are bridged by $\mu_3$-$O_{hydroxyl}$ atoms with Cu(1)···Cu(1a) distance of 2.990(2) Å to generate a butterfly-like tetranuclear $Cu_4(OH)_2Br_2(CO_2)_2$ cluster, in which Cu(1) and Cu(2) can function as body and wing, respectively (Supporting Information, Figure S3a). The edge-shared Cu(4) and Cu(5) dimer with Cu(4)···Cu(5) distance of 2.9739(19) Å is linked to the Cu(3) site through $\mu_3$-OH group via vertex-sharing mode to form a triangle trimer, two of which connect with each other by edge-sharing mode; the result is a steplike hexanuclear $Cu_6(OH)_4(CO_2)_4$ core (Supporting Information, Figure S3b). In **1**, both $Cu_4(OH)_2Br_2(CO_2)_2$ and $Cu_6(OH)_4(CO_2)_4$ clusters can be viewed as six-connected SBUs. Each $Cu_4(OH)_2Br_2(CO_2)_2$ cluster is linked to four $Cu_6(OH)_4(CO_2)_4$ clusters and two


dx.doi.org/10.1021/ic5001232 | Inorg. Chem. 2014, 53, 4130−4143

$Cu_4(OH)_2Br_2(CO_2)_2$ clusters, while each $Cu_6(OH)_4(CO_2)_4$ cluster is connected to four $Cu_4(OH)_2Br_2(CO_2)_2$ clusters and two $Cu_6(OH)_4(CO_2)_4$ clusters (Figure 1b,c). Notably, the linkers are single $\mu_3$- and double $\mu_2$-ina groups (Scheme 1a,b). The

**Scheme 1. The Coordination Modes of Ina Group in the Complexes 1−9**

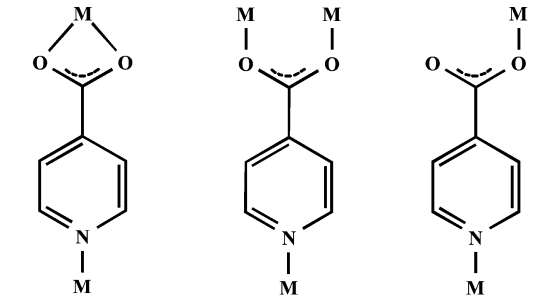


overall structure of **1** features a three-dimensional (3D) hexagonal MOF constructed by butterfly-like $Cu_4(\mu_3\text{-}OH)_2Br_2$ and steplike $Cu_6(\mu_3\text{-}OH)_4$, two different SBUs with the ratio of 1:1, possessing two different channels (Figure 1d,e). The topology analysis via Topos40 program suggests an $\alpha$-Po net of double nodes with the $(4^{12}\cdot6^3)$ topology symbol (Figure 1f). Isostructural **2** has cell volume slightly smaller than that of **1** due to chlorides in place of bromides (Supporting Information, Figure S4).

Compared to complex **2**, the generation of **3** with only butterfly-like $Cu_4(OH)_2Cl_2(CO_2)_2$ units as six-connected nodes can mainly be ascribed to the systematic variation of pH value by introducing auxiliary oxalate acid and changing the amount of reactants. Complex **3** crystallizes in the symmetrically higher monoclinic space group $P2_1/n$. There are only two crystallographically independent Cu(II) atoms, two ina ligands, one $\mu_3$-OH group, and one chloride in the asymmetric unit (Figure 2a). However, the Cu(1) and Cu(2) sites are also located in the general position and separately show Jahn−Teller distorted octahedral and square pyramidal coordination geometries. The Cu−O, Cu−N, and Cu−Cl distances are in the ranges of 1.9389(13)−2.1854(14) Å, 1.9922(16)−1.9955(15) Å, and 2.3454(5)−2.6518(5) Å, respectively. The cis and trans angles of L−Cu(1)−L (L = O, N, and Cl) are in the range of 78.45(4)−113.50(5)° and 151.44(4)−177.88(6)°. The Cu−O−Cu angles are in the range of 96.59(5)−124.13(6)°, and the Cu(2)−Cl(1)−Cu(1) angle is 75.431(14)°, respectively. Therefore, two edge-shared dimers from Cu(1) and Cu(2) are also bridged by $\mu_3$-$O_{hydroxyl}$ and $\mu_2$-Br atoms to generate a butterfly-like tetranuclear $Cu_4(OH)_2Cl_2(CO_2)_2$ cluster with Cu(2)···Cu(2b) distance of 2.9729(4)Å, in which the inversion center is situated in the body center (Supporting Information, Figure S5). Each butterfly-like $Cu_4(OH)_2Cl_2(CO_2)_2$ unit is bridged to six neighbors via eight ina groups to form a 3D hexagonal MOF with pcu topology (Figure 2b,c).

A similar reaction to **2** with the decrease of NaOH amount in starting materials can generate the linear $Cu_3(OH)_2(CO_2)_2$

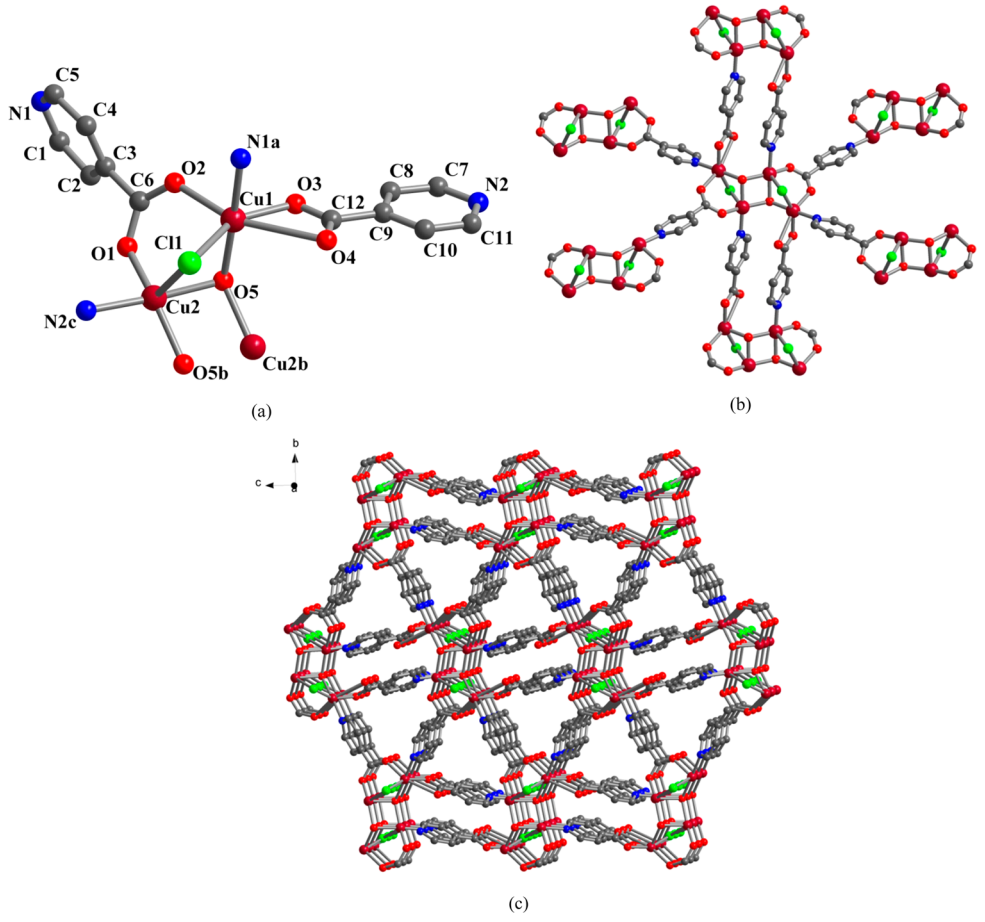


**Figure 2.** The coordination environment of Cu(II) ions (a), the connection modes of butterfly-like $Cu_4(OH)_2Br_2(CO_2)_2$ clusters (b), and 3D tetranuclear copper SBUs based hexagon MOF (c) in complex **3**.


dx.doi.org/10.1021/ic5001232 | Inorg. Chem. 2014, 53, 4130−4143

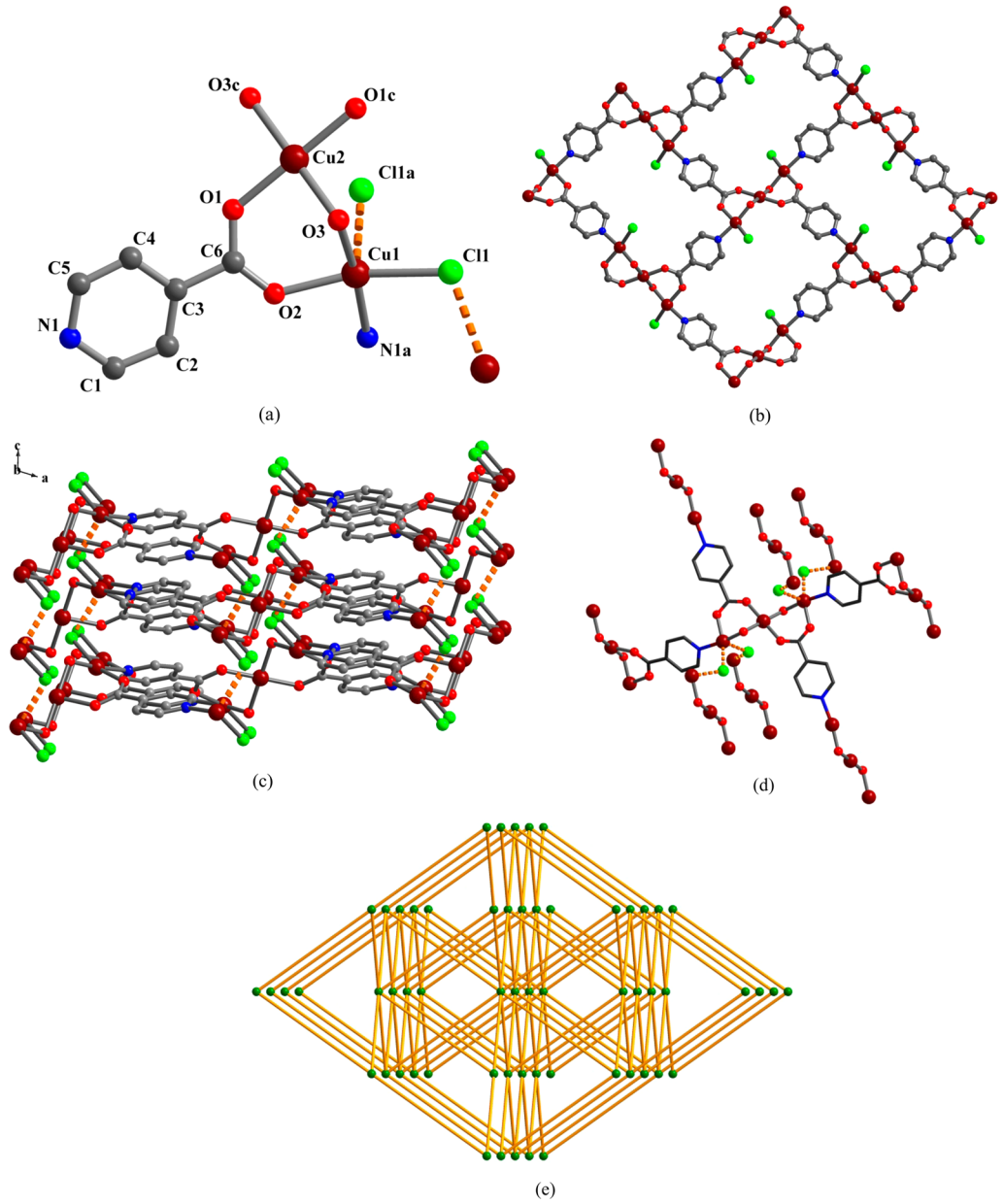


**Figure 3.** The coordination environment of Cu(II) ions (a), 2D wavelike (4,4) topological layer (b), 3D network based on 2D layer and Cu(1)···Cl(1b) weak interaction (c), the connection modes of $Cu_3(OH)_2(CO_2)_2$ core (d), and 3D eight-connected topological net(e) in complex **4**. The dashed lines represent weak Cu···Cl bonds.

cluster-based complex **4**. In contrast to the triclinic space group $P\bar{1}$ in **2**, complex **4** crystallizes in symmetrically higher monoclinic $P2_1/c$ space group, and the asymmetric unit contains two crystallographically independent Cu(II) ions, one ina group, one $\mu_2$-OH group, and one chloride (Figure 3a). Considering weaker and longer bond with Cu(1)···Cl(1a) distance of 2.6744(9) Å, Cu(1) atom has a distorted square pyramidal geometry of 4 + 1 constructed by two chlorine atoms, one $\mu_2$-$O_{hydroxyl}$ atom, one pyridine nitrogen atom, and one bis(monodentate) carboxylate oxygen atom. The Cu(2) site lies on the inversion center with the position occupancy of 0.5 and shows a square geometry formed by two $\mu_2$-$O_{hydroxyl}$ atoms and two bis(monodentate) carboxylate oxygen atoms. The Cu−O distances are in the range of 1.918(2)−1.996(2) Å; the Cu−N and Cu−Cl distances are separately 2.066(3) Å and 2.3106(9) Å. The cis and trans angles of L−Cu(1)−L (L = O, N, and Cl) are in the ranges of 86.37(10)−101.86(8)° and 163.12(8)−180.00(15)°, respectively. The Cu(1) and Cu(2) atoms are bridged by $\mu_2$-$O_{hydroxyl}$ atom and syn−syn carboxylate group to form a linear vertex-sharing $Cu_3(OH)_2(CO_2)_2$trimer with Cu−Cu distance of 3.159 Å and Cu(1)−O(3)−Cu(2) angle of 110.31(10)° (Supporting Information, Figure S6). The bridged $\mu_3$-ina groups link trinuclear $Cu_3(OH)_2(CO_2)_2$ cluster SBUs into a two-dimensional (2D) wavelike (4,4) topological layer (Scheme 1b and Figure 3b). Note that adjacent layers are further connected via weak Cu(1)···Cl(1a) bonds to yield 3D network in which each linear $Cu_3(OH)_2(CO_2)_2$ cluster is linked to its eight equivalents via four chlorides and four $\mu_3$-ina groups (Figure 3c,d). The topology analysis suggests that the whole structure features an eight-connected net with topology symbol of $(4^{24}\cdot6^4)$ by possessing linear $Cu_3(OH)_2(CO_2)_2$ core as node (Figure 3e). Isostructural **5** has cell volume slightly larger than that of **4** due to bromides in place of chlorides


dx.doi.org/10.1021/ic5001232 | *Inorg. Chem.* 2014, 53, 4130−4143

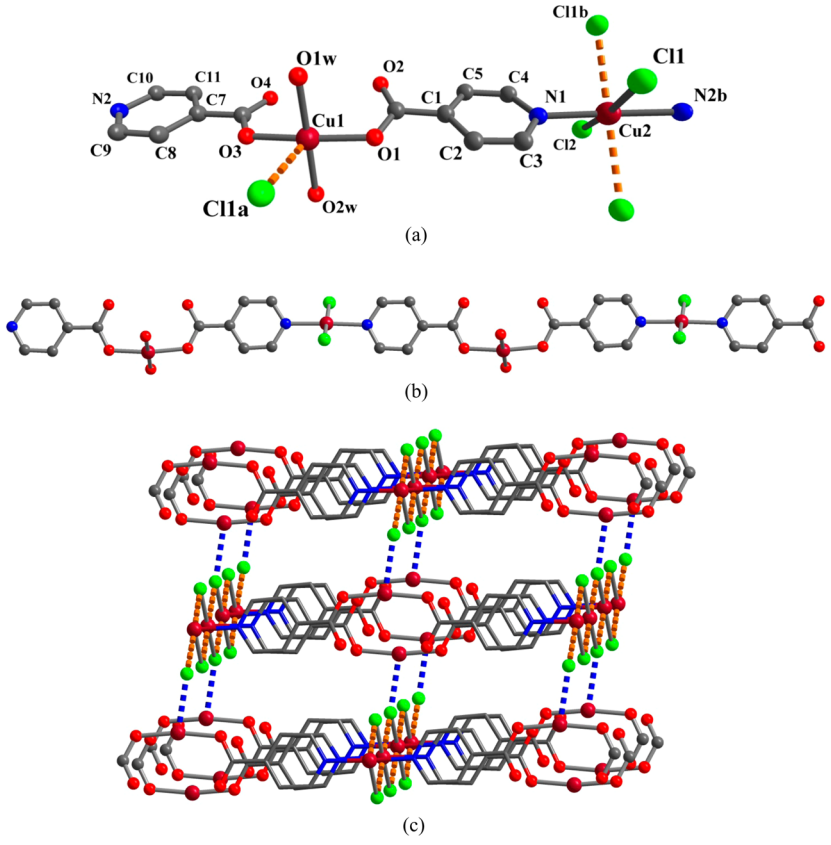


**Figure 4.** The coordination environment of Cu(II) ions (a), metal−organic Cu(II)-ina chain (b), and 3D supramolecular network constructed by weak Cu···Cl bonds (c) in complex **6**. The dashed lines in (c) represent weak Cu···Cl bonds. For clarity, the water molecules in (c) are omitted.

(Supporting Information, Figure S7). Different from the normal coordination bonds in **1**−**3**, the occurrence of weak Cu···X bonds may indicate that complexes **4**−**7** are the transition from MOF to SCC.

With the replacement of NaOH by $[N(Me)_4]Cl$ in the synthesis of **4**, hydroxyl-absent metal−organic coordination chain-based complex **6** was produced. The asymmetric unit consists of two crystallographically independent Cu(II) atoms, two ina groups, two chlorides, and two coordinated water molecules (Figure 4a). Both Cu(II) atoms lie on the general position and show slightly distorted square geometry. The Cu(1) site is coordinated by two monodentate carboxylate oxygen atoms and two terminal water molecules, while the Cu(2) site is ligated by two chlorine atoms and two pyridine nitrogen atoms. The Cu−O, Cu−N, and Cu−Cl distances are separately in the ranges of 1.941(2)−1.950(3) Å, 2.013(3)−2.017(3) Å, and 2.3051(10)−2.3233(9)Å, while the cis and trans angles of L−Cu−L (L = N, O, and Cl) are in the ranges of 85.69(9)−103.87(9)° and 132.88(4)−178.10(12)°, respectively. Two monodentate carboxylate oxygen atoms in $\mu_2$-ina groups are coordinated to the Cu(1) site in head-to-head mode, and two pyridine nitrogen atoms are coordinated to the Cu(2) site in end-to-end mode, yielding an infinite metal−organic coordination chain (Scheme 1c and Figure 4b). In fact, Cu(1) and Cu(2) atoms are additionally bonded to one and two Cl atoms via weak Cu···Cl bonds with distance of 2.69−2.86 Å, respectively, and thus they can be viewed as distorted square pyramid geometry of 4 + 1 and elongated octahedral geometry of 4 + 2. Then, infinite metal−organic chains are extended into (3,4)-connected supramolecular network via Cu−Cl weak interactions (Figure 4c).

With hydroxyacetic acid (Hgca) instead of the oxalate acid additive in the synthesis of **3**, metal−organic coordination ladder-based complex **7** was formed, in which the gca group serves not only as the mediator of pH value but also as auxiliary ligand coordinated to Cu(II) ions. There are two crystallographically independent Cu(II) ions, two ina groups, one gca group, one chloride, and one coordinated water molecule in the asymmetric unit of **7** (Figure 5a). The square pyramidal geometry of the Cu(1) site is generated from one hydroxyl oxygen atom and one bis(monodentate) carboxylate atom from the same one gca group, two monodentate carboxylate oxygen atoms from two ina groups, and one water molecule. The Cu(2) site adopts a slightly distorted square pyramidal configuration of 4 + 1 mode formed by one chlorine atom, one bis(monodentate) carboxylate oxygen atom from the gca group, and two pyridine nitrogen atoms. The Cu−Cl bond distance is 2.2666(7) Å, the Cu−O and Cu−N distances are in the ranges of 1.9498(17)−2.2424(18) Å and 2.0127(17)−2.0167(18) Å, while the cis and trans angles of L−Cu(2)−L (L = N, Cl, and O) are in the ranges of 79.23(6)−99.00(7)° and 169.46(8)−178.29(8)°, respectively. The bridged ina group in **7** shows the same coordinated mode as in **6**. However, the Cu(1) and Cu(2) sites are bridged via $\mu_2$-ina and $\mu_2$-gca groups to produce a ladder-shaped metal organic ribbon (Figure 5b). Adjacent ribbons are further extended via Cu(2)···Cl(1a) weak interactions of 2.835 Å into a supramolecular layer (Figure 5c).

In situ reduction of Cu(II)-to-Cu(I) could be realized by tuning reaction conditions. The formation of mixed-valent copper complex **8** can be promoted by increasing reaction temperature from 130 to 140 °C and using reducing MeOH instead of MeCN. One of the most outstanding features of **8** is


dx.doi.org/10.1021/ic5001232 | Inorg. Chem. 2014, 53, 4130−4143

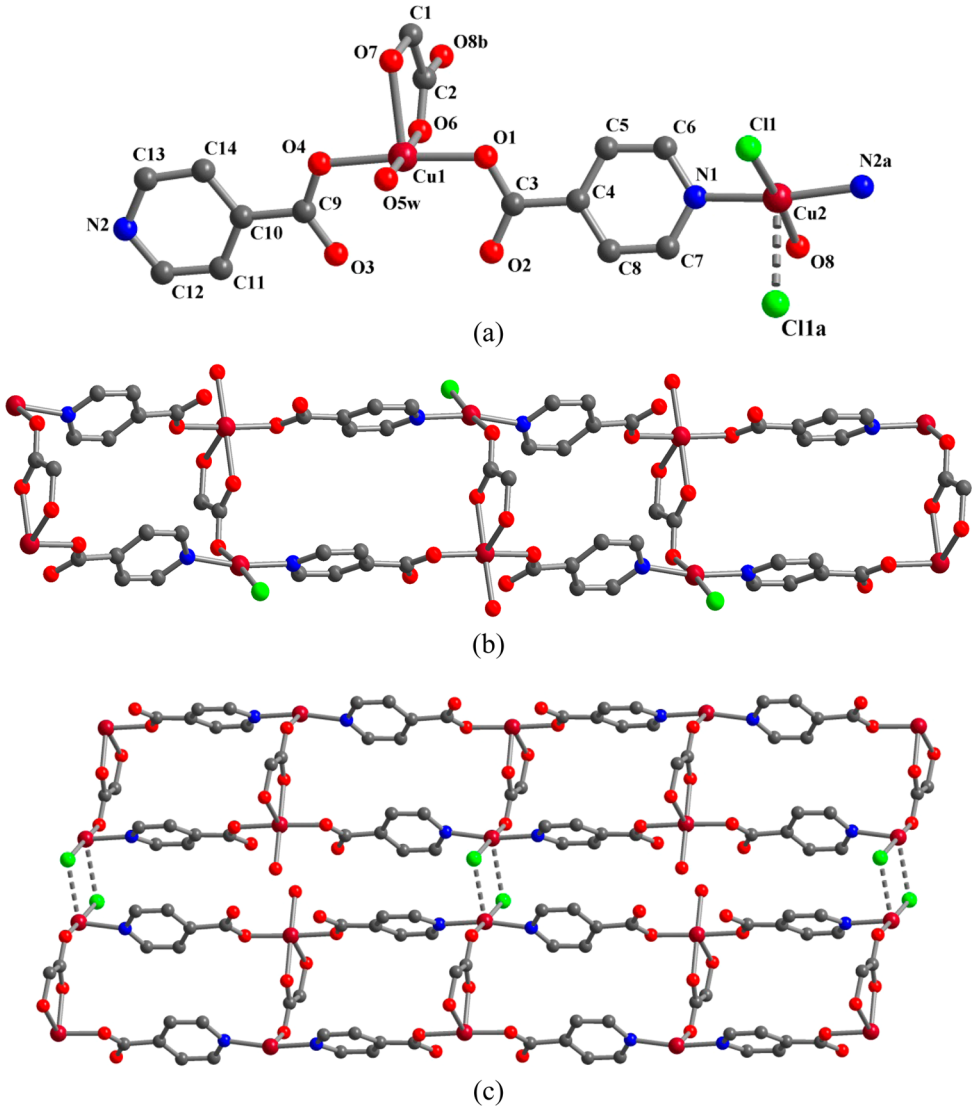


**Figure 5.** The coordination environment of Cu(II) ions (a), ladder (b), and 2D supramolecular layer (c) of complex **7**. The dashed lines in (c) represent weak Cu···Cl bonds.

the coexistence of two discrete units with opposite charges in 3D supramolecular network. **8** crystallizes in the monoclinic group $P2_1/c$, and the asymmetric unit consists of six crystallographically independent Cu atoms, seven bromine atoms, two N-methylated ina groups and one water molecule (Figure 6a). The Me-ina group came from in situ N-methylation reaction of ina and MeOH under higher temperature and alkaline condition. The Cu(1) atom is divalent, adopting a slightly distorted square pyramidal geometry coordinated by one water oxygen atom at the apical position and four bis(monodentate) carboxylate oxygen atoms in the equatorial plane. The Cu(1)−O distances are in the range of 1.935(8)−2.149(10) Å, while the cis O−Cu(1)−O angles are in the range of 88.6(4)−102.7(4)° and the trans O(2)−Cu(1)−O(1c) angle is 167.1(4)°. The monovalent Cu(2) to Cu(6) atoms exhibit similar distorted $CuBr_4$ tetrahedral coordination geometry. The Cu(I)−Br distances are in the range of 2.383(3)−2.831(19) Å and the angles of Br−Cu(I)−Br are in the range of 95.07(10)−129.32(13)°. The weak interactions between Cu(I) atoms vary from 2.729(3) to 2.954(13) Å, while the cis and trans angles of Cu···Cu···Cu are in the ranges of 60.27(16)−102.52(11)° and 139.97(12)−147.66(12)°, respectively.

Two divalent Cu(1) atoms with Cu(II)···Cu(II) distance of 2.673(3) Å are linked via four syn−syn carboxylates from Me-ina groups to give a paddlewheel-like $[Cu(Me\text{-}ina)_2]^{2+}$ unit (Supporting Information, Figure S8a). Five monovalent Cu atoms are bridged via $\mu_2$, $\mu_3$, and $\mu_4$ bromides to generate a cubane-based $[Cu_5Br_7]^{2-}$ chain in which the cubane structure is constructed by Cu(2), Cu(3), Cu(4), Cu(6), Br(1), Br(2), Br(3), and Br(7) atoms (Figure 6b). Two adjacent cubanes are held together by shared Cu(5) atom and bridged $\mu_2$ Br(6) atoms to form a double chairlike unit (Supporting Information, Figure S8b). The $[Cu_5Br_7]^{2-}$ chains are templated by paddlewheel-like $[Cu(Me\text{-}ina)_2]^{2+}$ cationic complexes and extend into 3D supramolecular array via C−H···$O_{water}$ and C−H···Br hydrogen bonds (Figure 6c). The cubane-based double chairlike unit in **8** is unique and unprecedented in the reported $[Cu_5X_7]^{2-}$ aggregate-based complexes.[22]

Zigzag $[Cu_2Br_3]^-$ chain-based cuprous SCC **9** was synthesized via replacement of mixed MeOH and water solvents in mixed valent **8** by pure MeOH. There are two crystallographically independent copper atoms, three bromine atoms, and one O-esterificated and N-methylated $Me_2$-ina group in the asymmetric unit (Figure 7a). Both Cu(1) and


dx.doi.org/10.1021/ic5001232 | Inorg. Chem. 2014, 53, 4130−4143

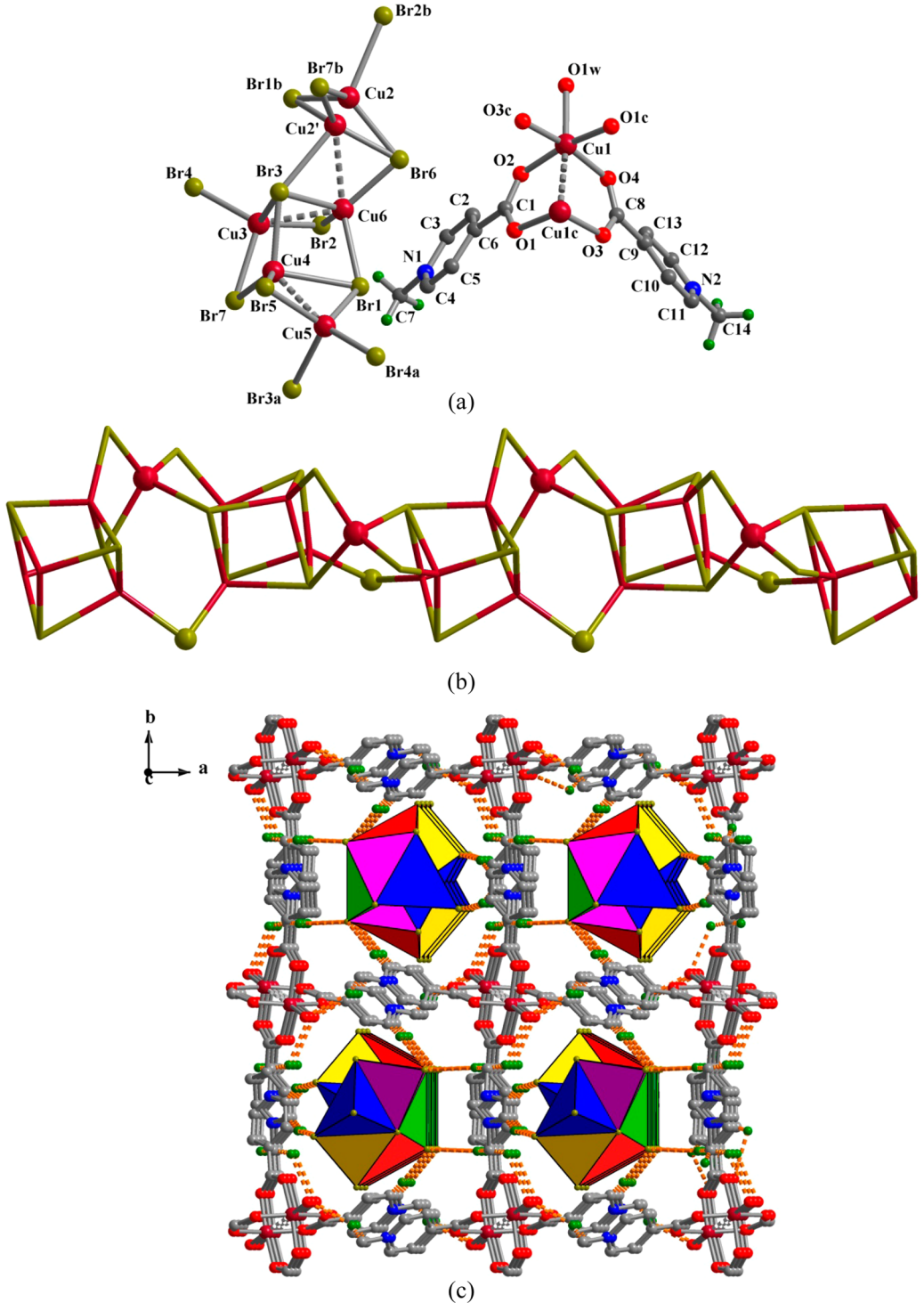


**Figure 6.** The coordination environment of Cu ions (a), cubane-based $[Cu_5Br_7]^{2-}$ chain (b), and 3D supramolecular array (c) in complex **8**. The C−H···O and C−H···Br hydrogen bonds are shown in dashed lines in (c).

Cu(2) atoms are monovalent and show distorted $CuBr_4$ tetrahedral geometry. The Cu−Br distances are in the range of 2.312(3)−2.798(4) Å, and the angles of Br−Cu−Br and Cu−Br−Cu are in the ranges of 53.05(9)−126.60(14)° and 52.77(9)−93.08(11)°, respectively. The edge- and face-shared connection of $CuBr_4$ tetrahedra generated a zigzag $[Cu_2Br_3]^-$ chain in which adjacent Cu(1)$Br_4$ or Cu(2)$Br_4$ tetrahedra are edge-shared, while Cu(1)$Br_4$ and Cu(2)$Br_4$ tetrahedra are face-shared (Figure 7b). The face-shared connection gave rise to very short Cu(I)−Cu(I) distance of 2.448(4) Å, which is shorter than the sum of the van der Waals radii of $Cu^I$ atoms (2.80 Å).[15c,23] What's more, the Cu(I)−Cu(I) distance of 2.448(4) Å is shorter than 2.556 Å in the open-shell metallic copper, indicating strong ligand-supported Cu···Cu interaction.[24] According to Pauling's rule, *the sharing of edges and particularly faces by two anion polyhedra decreases the stability of an ionic structure*. Thus, the edge- and face-shared $[Cu_2Br_3]^-$ chain is energetically unfavorable, which is stabilized by


dx.doi.org/10.1021/ic5001232 | *Inorg. Chem.* 2014, 53, 4130−4143

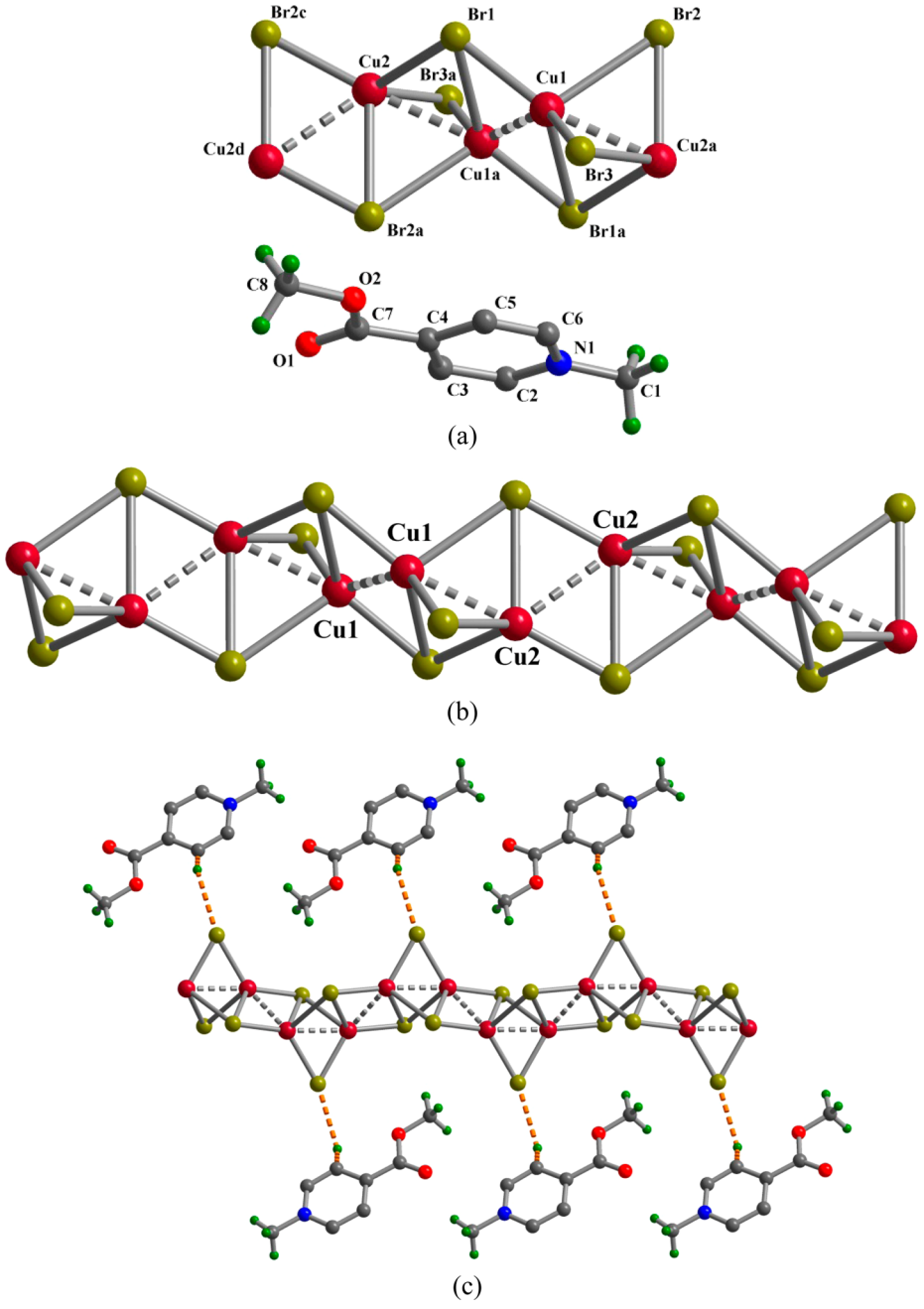


**Figure 7.** The coordination environment of Cu(I) ions (a), alternate face- and edge-shared $[Cu_2Br_3]^-$ chain (b), and supramolecular array (c) in complex **9**.

O-esterificated and N-methylated $[Me_2\text{-ina}]^+$ templates via C−H···Br interactions to generate a ribbonlike supramolecular array (Figure 7c). The presence of organic $[Me_2\text{-ina}]^+$ templates rather than $[Cu(Me\text{-ina})_2]^{2+}$ complex makes complex **9** quite different from **8**. The generation of cuprous bromide aggregates promotes the occurrence of C−H···Br hydrogen bonds. It indicates the structures of **8** and **9** turned into supramolecular array.

**Magnetic Properties.** Magnetic susceptibility measurements for **1**, **3**, **4**, **6**, and **7** were performed with direct current (dc) field of 1000 Oe between 1.8 and 300 K on a Quantum Design SQUID MPMS XL-5. The magnetic behavior of **1** is shown in Figure 8. At room temperature, the $\chi_mT$ product per $Cu_5$ unit of 2.795 $cm^3$ K $mol^{-1}$ is already higher than 1.875 $cm^3$ K $mol^{-1}$ for five uncoupled $Cu^{II}$ ions ($S = 1/2$). As the temperature decreases, the $\chi_mT$ product climbs steadily up to 20 K and then rapidly reaches maxima of ca. 135.35 $cm^3$ K $mol^{-1}$ at 7 K, indicating dominant intracluster ferromagnetic (FO) interactions, while the final decline at low temperature suggests the presence of intercluster antiferromagnetic (AFM) interactions. To have a qualitative view of the dominant interactions present in the system, a Curie−Weiss analysis of magnetic susceptibility data by $\chi_m = C/(T - \theta)$ in the high-temperature (30−300 K) region gave a Curie constant of $C$ = 2.604 $cm^3$ K $mol^{-1}$ and Weiss constant of $\theta$ = +19.88 K (Figure 8, inset). The magnetization of **1** at 2 K rapidly increases, reaching saturation value of 5.2485 N$\beta$ at 50 KOe, which is close to the theoretical value of 5 N$\beta$ expected for five ferromagnetically coupled Cu(II) centers. Field-cooled (FC) and zero-field-cooled (ZFC) magnetizations were performed under an applied field of


dx.doi.org/10.1021/ic5001232 | Inorg. Chem. 2014, 53, 4130−4143

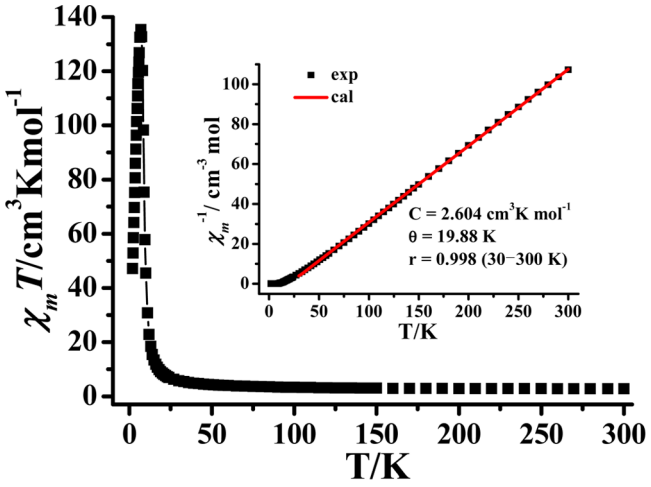


**Figure 8.** $\chi_m T$ vs $T$ plot for complex **1**. (inset) Curie–Weiss fitting of $\chi_m^{-1}$ vs $T$ plot of **1**, experimental (black) and calculated (red).

10 Oe, and the bifurcation at 8 K indicates the onset of long-range magnetic ordering (Supporting Information, Figure S10). Because of the Cu–O–Cu angles in the range of 95.9(2)–126.8(3)°, the principal magnetic interactions in **1** between metal centers can be easily rationalized according to the geometry around the copper atoms and the superexchange pathways via $\mu_3$-hydroxyl, $\mu_2$-bromide, and carboxylate bridges.[25]

For **3**, the $\chi_m T$ product at 300 K per $Cu_2$ unit is 0.86 $cm^3$ K $mol^{-1}$, which is close to the expected value 0.75 $cm^3$ K $mol^{-1}$ of two spin-only Cu(II) ions, corresponding to an average $g$ factor of 2.14. Upon cooling, the $\chi_m T$ product decreases gradually to a minimum of 0.0504 $cm^3$ K $mol^{-1}$ at 20 K, then rises abruptly to a maximum of 0.4405 $cm^3$ K $mol^{-1}$ at 6 K, and finally drops to 0.0325 $cm^3$ K $mol^{-1}$ at 2 K. The minimum at 20 K indicates a spin canting antiferromagnetic behavior, which is supported by the fact that the maximum $\chi_m T$ at low temperature is lower than that at room temperature (Figure 9). The magnetization

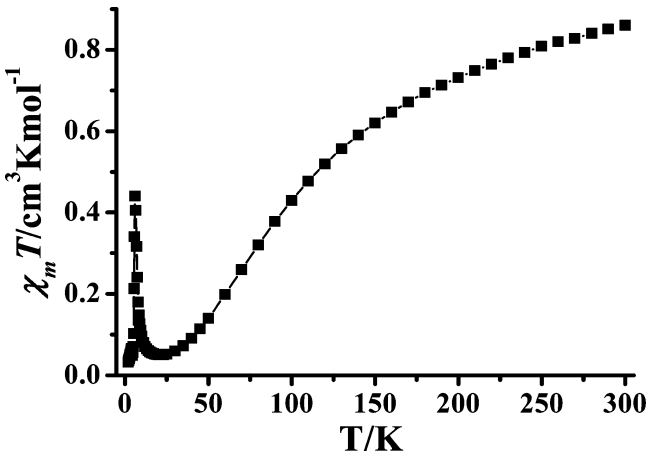


**Figure 9.** $\chi_m T$ vs $T$ plot for complex **3**.

of **3** at 2 K slowly increases with the applied field, and no saturation is reached at 50 000 Oe, which is also a characteristic of an antiferromagnet. The bifurcation at 8 K in FC–ZFC magnetizations under an applied field of 10 Oe indicates the onset of long-range magnetic ordering (Supporting Information, Figure S11). The magnetic interactions in **1** and **3** are not limited to intracopper clusters, and weak interactions between clusters can propagat via ina groups. We could not get a suitable model to fit measured data.

At room temperature, the $\chi_m T$ product per $Cu_3$ unit for **4** is 1.542 $cm^3$ K $mol^{-1}$, which is already larger than the expected spin-only value of 1.125 $cm^3$ K $mol^{-1}$ for three Cu(II) atoms taking $g = 2$ and $S = 1/2$. As the temperature decreases, the $\chi_m T$ product climbs steadily up to 20 K and then rapidly reaching maxima of ca. 32.39 $cm^3$ K $mol^{-1}$ at 6.5 K, indicating dominant intracluster FO interactions.[26] The final decline of the $\chi_m T$ product at low temperature suggests the presence of intercluster AFM interactions (Figure 10). The magnetization

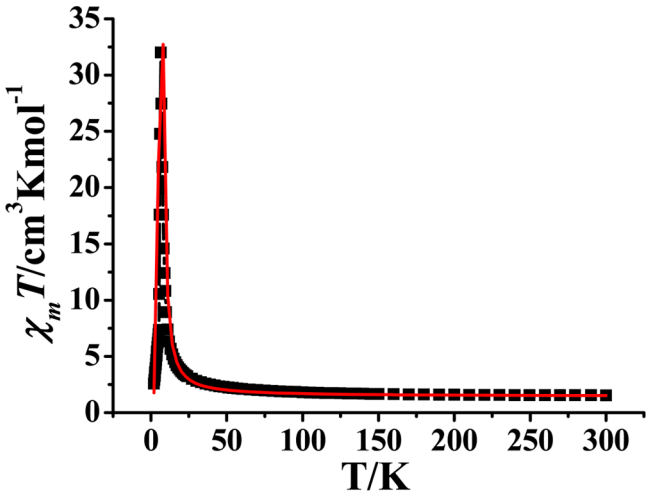


**Figure 10.** Experimental (black) and simulated (red) $\chi_m T$ vs $T$ and $\chi_m^{-1}$ vs $T$ plots for complex **4**.

of complex **4** at 2 K rapidly increases and reaches saturation value of 3.0585 N$\beta$ at 50 KOe, which is close to the theoretical value of 3N$\beta$ for a ferromagnetic $Cu_3$ unit. FC–ZFC magnetizations performed under an applied field of 10 Oe show a bifurcation at 8 K (Supporting Information, Figure S12). From the relatively simple structure of **4**, the magnetic data was fitted by a linear trinuclear system. The detailed Heisenberg Hamiltonian and the derivation of theoretical equations of magnetic susceptibility are listed in Scheme 2. As the two terminal

**Scheme 2. The Detailed Heisenberg Hamiltonian and the Derivation of Theoretical Equations of Magnetic Susceptibility of Complex 4**

$$H = -J(S_{Cu2Cu1} + S_{Cu2Cu1c})$$

$$\chi_{trimer} = \frac{3e^{0.75J/kT} + 3e^{-1.25J/kT} + 30e^{1.75J/kT}}{4e^{0.75J/kT} + 4e^{-1.25J/kT} + 8e^{1.75J/kT}} \times \frac{N\beta^2 g^2}{3k(T-\theta)}$$

$$\chi_M = \frac{\chi_{trimer}}{1 - \frac{2zJ'}{\beta^2 g^2} \times \chi_{trimer}} + TIP$$

copper atoms are symmetry-related, only one coupling constant, $J$, is involved. The best fitting at 2–300 K upon the Cu1-$J$-Cu2-$J$-Cu1 mode with the consideration of other factors gives $J = 1.8079$ $cm^{-1}$, $g = 2.25$, TIP = $3.899 \times 10^{-5}$ $cm^3$ mol, $\theta = +37.4963$ K, $zJ' = -10.858\,93$, where $J$ is a coupling constant, $\theta$ is other factors, $g$ is the Zeeman factor, and TIP is the temperature-independent paramagnetism. This indicates that the Cl bridges in Cu(1)···Cl(1b)


dx.doi.org/10.1021/ic5001232 | Inorg. Chem. 2014, 53, 4130–4143

weak bonds also played an indispensable role in the magnetic superexchange. According to the linear correlation of $J$ ($cm^{-1}$) = $-74\ \alpha$ (degrees of Cu−O−Cu) + 7270, a Cu−O−Cu angle larger than 97° often shows antiferromagnetic interaction between the metal ions.[27] Complex **3** still shows ferromagnetic behavior in spite of Cu(1)−O(3)−Cu(2) angle of 110.31(10)°. This can be easily explained by the environment around the Cu(II) ion in the hydroxyl-bridged dimeric unit. Eliminating weak Cu···Cl interaction in **4**, the $Cu_3$ trimer unit comprises one square and two tetrahedral Cu(II) ions. Their single magnetic orbitals are $a_1(d_{xy})$, $a_2(d_{yz})$ and $b_2(d_{zx})$, and the final magnetic interactions are $J = J_{a1b1}$, $J_{a2b1}$, and $J_{b2b1}$, where all the $J_{a1b1}$, $J_{a2b1}$, and $J_{b2b1}$ terms are strictly positive, then ferromagnetic interactions are expected. It is well-consistent with the experimental results.[9c]

For **6**, the $\chi_m T$ value at 300 K is 0.9878 $cm^3$ K $mol^{-1}$, which is close to the expected value (0.75 $cm^3$ K $mol^{-1}$, taking $g = 2$) for the $Cu_2$ unit ($S = 1/2$). When complex **6** is cooled, the $\chi_m T$ product continuously decreases and reaches the value of 0.0436 $cm^3$ K $mol^{-1}$ at 2 K, characteristic of strong AFM interactions between $Cu^{II}$ spin carriers (Figure 11). The field-dependent

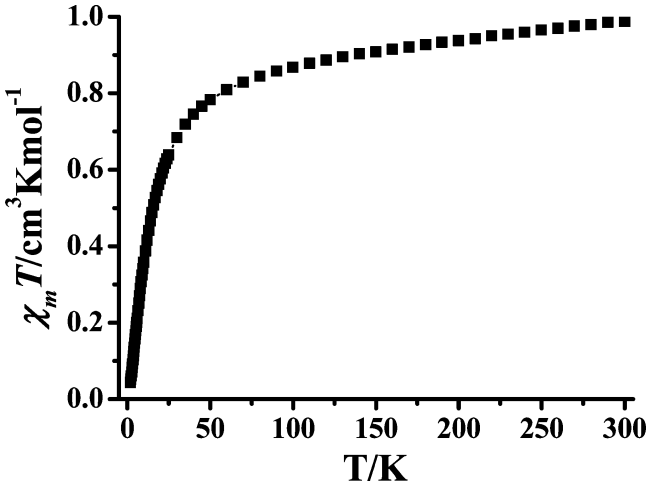


**Figure 11.** Plot of $\chi_m T$ versus $T$ for complex **6**.

magnetization at 2 K increases slowly and linearly with the applied field, and no saturation is observed. The magnetization value at the highest field, 50 KOe, is 0.2853 N$\beta$, far below the saturation value of 2 N$\beta$ expected for two spin-only Cu(II) species (Supporting Information, Figure S13a).

For **7**, the $\chi_m T$ product per $Cu_2$ unit at room temperature is 1.0273 $cm^3$ K $mol^{-1}$, which is higher than the expected spin-only value of 0.75 $cm^3$ K $mol^{-1}$, taking $g = 2$ and $S = 1/2$ (Figure 12). As the temperature decreases, the $\chi_m T$ product remains constant up to 20 K and then rapidly decreases to the value of 0.3903 $cm^3$ K $mol^{-1}$ at 2 K, demonstrating paramagnetic interactions between $Cu^{II}$ spin carriers. The magnetization value of complex **7** at 2 K increases linearly with the applied field (Supporting Information, Figure S13b).

**Photoluminescent Properties.** The photoluminescent properties of **8** and **9** with novel cuprous bromide motifs were studied in the solid state at room temperature. Complex **8** shows a blue emission at 438 nm (Figure 13a). In general, possible assignments for the excited states that are responsible for emissions of Cu(I) complexes are ligand-centered transitions (LC), ligand-to-ligand (LLCT), ligand-to-metal (LMCT), metal-to-ligand (MLCT) charge transfer transitions, or metal-center $d^{10}\rightarrow d^9s^1$ (MC) transitions.[28] From the survey

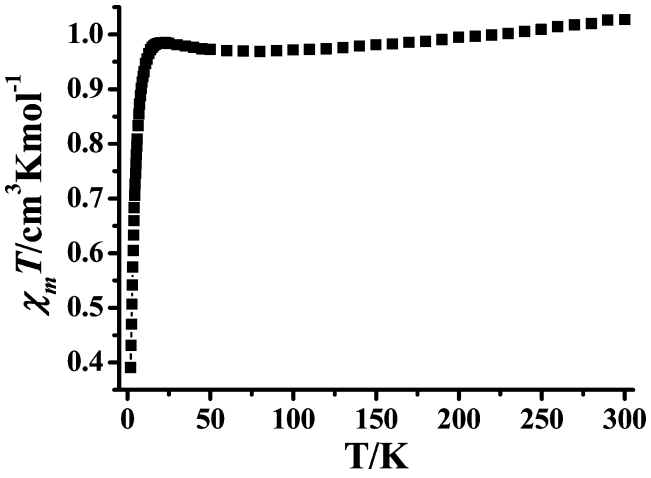


**Figure 12.** Temperature dependence of $\chi_m T$ per $Cu_2$ unit for complex **7**.

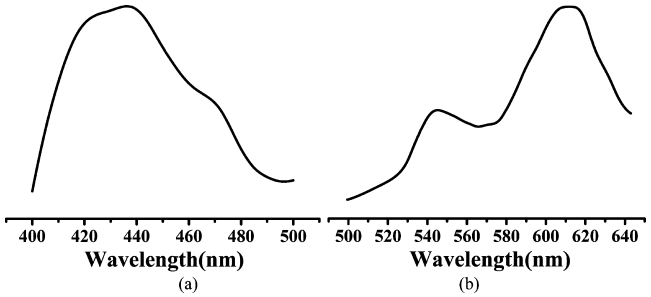


**Figure 13.** Photoluminescent emissions of (a) complex **8** upon excitation at 374 and 394 nm and (b) complex **9** upon excitation at 220 nm.

of lots of literature, the emission band centered at 438 nm may be assigned as originating from a bromine-to-copper transition (XMCT). Different from **8**, complex **9** exhibits a stronger red emission at 613 nm and a weaker green emission at 544 nm upon excitation (Figure 13b). According to the photoluminescent properties of known Cu···Cu interacted complexes of cuprous halides, the stronger orange photoluminescence is possibly assigned to the charge transfer from metal-center transition in copper cluster (MC), and the weaker green emission is possibly assigned as originating from a ligand-to-copper transition (LMCT).[18b,29]

## ■ CONCLUSIONS

In summary, nine novel Cu(II), Cu(I,II), and Cu(I) compounds were solvothermally produced from starting materials of copper halides by changing reaction conditions such as temperature, pH value, solvent, reactant ratio, and additives. Nine complexes can be classified as three types according to bonding types of halides: cupric complexes **1**−**3** include only the normal X−Cu bond; cupric complexes **4**−**7** include the normal X−Cu bond and a weak X···Cu bond; mixed-valent complex **8** and cuprous complex **9** include the normal X−Cu bond and C−H···X halogen hydrogen bonds. A series of SBUs including linear $Cu_3(OH)_2$ timer, butterfly-like $Cu_4(\mu_3\text{-}OH)_2X_2$, and steplike $Cu_6(\mu_3\text{-}OH)_4$ were revealed, and ferromagnetic, spin canting antiferromagnetic, and paramagnetic interactions have been observed. A variety of topological nets such as six-connected pcu, four-connected (4,4) net, eight-connected net, and (3,4)-connected layer were observed. Novel cubane-containing $[Cu_5Br_7]^{2-}$ chain and face-sharing tetrahedra-based


dx.doi.org/10.1021/ic5001232 | Inorg. Chem. 2014, 53, 4130−4143

$[Cu_2Br_3]^-$chain was discovered. N-methylation and O-esterification of ina group occurred in situ. Nine complexes show gradual transitions of valence ($Cu^{II} \rightarrow Cu^{I,II} \rightarrow Cu^{I}$), bonding types (X−Cu bond → X···Cu weak bond → C−H···Br halogen bond), hierarchical structures (typical coordination polymer → weak X···Cu bond contained coordination polymer → SCC), and physical properties (magnetism → luminescence).

## ■ ASSOCIATED CONTENT

### Supporting Information

Additional figures in CIF format, tables of selected bonds, IR spectra, PXRD patterns, and magnetism curves for complexes **1**−**9**. This material is available free of charge via the Internet at http://pubs.acs.org.

## ■ AUTHOR INFORMATION


### Corresponding Author

*E-mail: zhangxm@dns.sxnu.edu.cn. Fax: +86 357 2051402.


### Notes

The authors declare no competing financial interest.

## ■ ACKNOWLEDGMENTS

This work was supported by the 973 Program (2012CB821701), the Ministry of Education of China (Grant IRT1156), and the National Science Fund for Distinguished Young Scholars (Grant 20925101).

## ■ REFERENCES


(1) (a) Cook, T. R.; Zheng, Y.-R.; Stang, P. J. *Chem. Rev.* **2012**, *113*, 734−777. (b) Eddaoudi, M.; Moler, D. B.; Li, H.; Chen, B.; Reineke, T. M.; O'Keeffe, M.; Yaghi, O. M. *Acc. Chem. Res.* **2001**, *34*, 319−330. (c) Zaworotko, M. J. *Angew. Chem., Int. Ed.* **2000**, *39*, 3052−3054.

(2) (a) Mroziński, J. *Coord. Chem. Rev.* **2005**, *249*, 2534−2548. (b) Peng, R.; Li, M.; Li, D. *Coord. Chem. Rev.* **2010**, *254*, 1−18. (c) Cui, Y.; Yue, Y.; Qian, G.; Chen, B. *Chem. Rev.* **2011**, *112*, 1126−1162.

(3) (a) Stock, N.; Biswas, S. *Chem. Rev.* **2011**, *112*, 933−969. (b) Chen, Q.; Xue, W.; Lin, J.-B.; Lin, R.-B.; Zeng, M.-H.; Chen, X.-M. *Dalton Trans.* **2012**, *41*, 4199−4206.

(4) (a) Willett, R. D. *Coord. Chem. Rev.* **1991**, *109*, 181−205. (b) Wei, M.; Willett, R. D. *Inorg. Chem.* **1996**, *35*, 6381−6385.

(5) (a) Solomon, E. I.; Sundaram, U. M.; Machonkin, T. E. *Chem. Rev.* **1996**, *96* (7), 2563−2606. (b) Noro, S.-i. *Phys. Chem. Chem. Phys.* **2010**, *12*, 2519−2531.

(6) (a) Wang, X.-Y.; Scancella, M.; Sevov, S. C. *Chem. Mater.* **2007**, *19*, 4506−4513. (b) Laborda, S.; Clérac, R.; Anson, C. E.; Powell, A. K. *Inorg. Chem.* **2004**, *43*, 5931−5943.

(7) (a) Maspoch, D.; Ruiz-Molina, D.; Wurst, K.; Domingo, N.; Cavallini, M.; Biscarini, F.; Tejada, J.; Rovira, C.; Veciana, J. *Nat. Mater.* **2003**, *2*, 190−195. (b) Dechambenoit, P.; Long, J. R. *Chem. Soc. Rev.* **2011**, *40*, 3249−3265. (c) Chivers, T.; Fu, Z.; Thompson, L. K. *Chem. Commun.* **2005**, *18*, 2339−2341.

(8) Ruiz, E.; Alemany, P.; Alvarez, S.; Cano, J. *J. Am. Chem. Soc.* **1997**, *119*, 1297−1303.

(9) (a) Ferrer, S.; Haasnoot, J. G.; Reedijk, J.; Müller, E.; Biagini Cingi, M.; Lanfranchi, M.; Manotti Lanfredi, A. M.; Ribas, J. *Inorg. Chem.* **2000**, *39*, 1859−1867. (b) Casarin, M.; Corvaja, C.; Di Nicola, C.; Falcomer, D.; Franco, L.; Monari, M.; Pandolfo, L.; Pettinari, C.; Piccinelli, F. *Inorg. Chem.* **2005**, *44*, 6265−6276. (c) Luo, F.; Che, Y.-x.; Zheng, J.-m. *Cryst. Growth. Des.* **2009**, *9*, 2047−2049.

(10) (a) El-Toukhy, A.; Cai, G. Z.; Davies, G.; Gilbert, T. R.; Onan, K. D.; Veidis, M. *J. Am. Chem. Soc.* **1984**, *106*, 4596−4605. (b) Canaj, A. B.; Tzimopoulos, D. I.; Philippidis, A.; Kostakis, G. E.; Milios, C. J. *Inorg. Chem.* **2012**, *51*, 10461−10470. (c) Liu, Q.-Y.; Yuan, D.-Q.; Xu, L. *Cryst. Growth Des.* **2007**, *7*, 1832−1843. (d) Lah, N.; Leban, I.; Clérac, R. *Eur. J. Inorg. Chem.* **2006**, *2006* (23), 4888−4894.

(11) Aromí, G.; Gamez, P.; Roubeau, O.; Kooijman, H.; Spek, A. L.; Driessen, W. L.; Reedijk, J. *Angew. Chem., Int. Ed.* **2002**, *41*, 1168−1170.

(12) Liu, X.; McAllister, J. A.; de Miranda, M. P.; Whitaker, B. J.; Kilner, C. A.; Thornton-Pett, M.; Halcrow, M. A. *Angew. Chem., Int. Ed.* **2002**, *41*, 756−758.

(13) (a) Charlot, M. F.; Jeannin, S.; Jeannin, Y.; Kahn, O.; Lucrece-Abaul, J.; Martin-Frere, J. *Inorg. Chem.* **1979**, *18*, 1675−1681. (b) Sarkar, B.; Ray, M. S.; Li, Y.-Z.; Song, Y.; Figuerola, A.; Ruiz, E.; Cirera, J.; Cano, J.; Ghosh, A. *Chem.—Eur. J.* **2007**, *13*, 9297−9309.

(14) Hong, M.-C.; Chen, L. *Design and Construction of Coordination Polymers;* Wiley Online Library: Hoboken, NJ, 2009.

(15) (a) Lu, J. Y. *Coord. Chem. Rev.* **2003**, *246*, 327−347. (b) Yaghi, O. M.; Li, H. *J. Am. Chem. Soc.* **1995**, *117*, 10401−10402. (c) Hao, Z.-M.; Wang, J.; Zhang, X.-M. *CrystEngComm* **2010**, *12*, 1103−1109.

(16) (a) Zhang, X.-M.; Tong, M.-L.; Chen, X.-M. *Angew. Chem., Int. Ed.* **2002**, *41*, 1029−1031. (b) Zhang, J.-P.; Zheng, S.-L.; Huang, X.-C.; Chen, X.-M. *Angew. Chem., Int. Ed.* **2004**, *43*, 206−209. (c) Willett, R. D. *Inorg. Chem.* **2001**, *40*, 966−971.

(17) (a) Wang, X.-L.; Qin, C.; Wang, E.-B.; Su, Z.-M.; Li, Y.-G.; Xu, L. *Angew. Chem., Int. Ed.* **2006**, *45*, 7411−7414. (b) Arnby, C. H.; Jagner, S.; Dance, I. *CrystEngComm* **2004**, *6*, 257−275.

(18) (a) Cheng, J.-K.; Yao, Y.-G.; Zhang, J.; Li, Z.-J.; Cai, Z.-W.; Zhang, X.-Y.; Chen, Z.-N.; Chen, Y.-B.; Kang, Y.; Qin, Y.-Y.; Wen, Y.-H. *J. Am. Chem. Soc.* **2004**, *126*, 7796−7797. (b) Hou, J.-J.; Li, S.-L.; Li, C.-R.; Zhang, X.-M. *Dalton Trans.* **2010**, *39* (10), 2701−2707.

(19) (a) Lu, J. Y.; Babb, A. M. *Chem. Commun.* **2001**, *9*, 821−822. (b) Lu, J. Y.; Babb, A. M. *Chem. Commun.* **2002**, *13*, 1340−1341. (c) Lin, C. Z. J.; Chui, S. S. Y.; Lo, S. M. F.; Shek, F. L. Y.; Wu, M.; Suwinska, K.; Lipkowski, J.; Williams, I. D. *Chem. Commun.* **2002**, *15*, 1642−1643.

(20) Chen, C.-L.; Beatty, A. M. *J. Am. Chem. Soc.* **2008**, *130* (51), 17222−17223.

(21) (a) Pilar, A. O.; Lorena, W.; Rodrigo, G. P.; Pablo, J. S. M.; Carlos, J. G. G.; Eva, M. M.; Salome, D.; Julio, G. H.; Félix, Z. *Chem. Commun.* **2010**, *46*, 3262−3264. (b) Bai, X.-L; Li, Y.-G.; Wang, E.-B.; Xu, L. *Inorg. Chem. Acta.* **2005**, *358*, 2571−2574.

(22) (a) Hartl, H.; Mahdjour-Hassan-Abadi, F. *Angew. Chem., Int. Ed.* **1984**, *23*, 378−379. (b) Hammond, R. P.; Chesnut, D. J.; Zubieta, J. A. *J. Solid State Chem.* **2001**, *158*, 55−60. (c) Chan, L. Y. Y.; Geller, S.; Skarstad, P. M. *J. Solid State Chem.* **1978**, *25*, 85−99. (d) Andersson, S.; Jagner, S. *J. Crystallogr. Spectrosc. Res.* **1988**, *18*, 591−600. (e) Hou, J.-J.; Guo, C.-H.; Zhang, X.-M. *Inorg. Chim. Acta* **2006**, *359*, 3991−3995.

(23) (a) Pyykkö, P. *Chem. Rev.* **1997**, *97*, 597−636. (b) Qin, Y.-L.; Liu, J.; Hou, J.-J.; Yao, R.-X.; Zhang, X.-M. *Cryst. Growth Des.* **2012**, *12*, 6068−6073. (c) Hao, Z.-M.; Guo, C.-H.; Wu, H.-S.; Zhang, X.-M. *CrystEngComm* **2010**, *12*, 55−58.

(24) Wing-Wah Yam, V.; Kam-Wing Lo, K. *Chem. Soc. Rev.* **1999**, *28*, 323−334.

(25) Mukherjee, P. S.; Maji, T. K.; Mostafa, G.; Ribas, J.; El Fallah, M. S.; Chaudhuri, N. R. *Inorg. Chem.* **2001**, *40*, 928−931.

(26) Liu, T.-F.; Fu, D.; Gao, S.; Zhang, Y.-Z.; Sun, H.-L.; Su, G.; Liu, Y.-J. *J. Am. Chem. Soc.* **2003**, *125*, 13976−13977.

(27) Kahn, O. *Molecular Magnetism;* Wiley-VCH: New York, 1993.

(28) Allendorf, M. D.; Bauer, C. A.; Bhakta, R. K.; Houk, R. J. T. *Chem. Soc. Rev.* **2009**, *38*, 1330.

(29) Liu, B.; Xu, L.; Guo, G. *J. Solid State Chem.* **2006**, *179*, 883−890.